Long-term modulations of Saturn's auroral radio emissions by the solar wind and seasonal variations controlled by the solar ultraviolet flux

T. Kimura, L. Lamy, C. Tao, S. Badman, S. Kasahara, B. Cecconi, P. Zarka, A. Morioka, Y. Miyoshi, D. Maruno, et al.

Long-term modulations of Saturn's auroral radio emissions by the solar wind and seasonal variations controlled by the solar ultraviolet flux

T. Kimura,[1] L. Lamy,[2] C. Tao,[1] S. V. Badman,[3] S. Kasahara,[1] B. Cecconi,[2] P. Zarka,[2] A. Morioka,[4] Y. Miyoshi,[5] D. Maruno,[6] Y. Kasaba,[6] and M. Fujimoto[1]

Received 26 March 2013; revised 6 October 2013; accepted 12 October 2013; published 14 November 2013.

[1] Saturn's auroral activities have been suggested to be controlled by the seasonal variations of the polar ionospheric conductivities and atmospheric conditions associated with the solar extreme ultraviolet (EUV) flux. However, they have not yet been explained self-consistently by only the seasonal solar EUV effects. This study investigates the long-term variations of Saturnian Kilometric Radiation (SKR) as a proxy of the auroral activities, which were observed by Cassini's Radio and Plasma Wave Science experiment mostly during the southern summer (DOY (day of year) 001 2004 to DOY 193 2010). We deduced the height distribution of the SKR source region in the Northern (winter) and Southern (summer) Hemispheres from the remote sensing of SKR spectra. The peak spectral density of the southern (summer) SKR was found to be up to 100 times greater than that of the northern (winter) SKR, and the altitude of the peak flux was similar ($\sim 0.8\ R_S$) in the Northern and Southern Hemispheres. The spectral densities in both hemispheres became comparable with each other around equinox in August 2009. These results suggest a stronger SKR source region during the summer than the winter related to the seasonal EUV effect, which is opposite to the trend observed in the Earth's kilometric radiation. A long-term correlation analysis was performed for the SKR, solar EUV flux, and solar wind parameters extrapolated from Earth's orbit by an magnetohydrodynamical simulation focusing on variations on timescales longer than several weeks. We confirmed clear positive correlations between the solar wind dynamic pressure and peak flux density in both the Southern and Northern Hemispheres during the declining phase of the solar cycle. We conclude that the solar wind variations on the timescale of the solar cycle control the SKR source region. In addition, it was also confirmed that the south-to-north ratios of SKR power flux and source altitudes are positively correlated with the solar EUV flux. This result strongly supports a seasonal EUV effect on the SKR source region. The variations of SKR activity over both seasonal and solar cycles are discussed in comparison to the terrestrial case.

Citation: Kimura, T., et al. (2013), Long-term modulations of Saturn's auroral radio emissions by the solar wind and seasonal variations controlled by the solar ultraviolet flux, *J. Geophys. Res. Space Physics*, *118*, 7019–7035, doi:10.1002/2013JA018833.

1. Introduction

[2] Auroral radio emissions are universal in all the magnetized planets and extremely intense, which implies that their generation must be a one-step process directly converting the free energy of auroral electrons into electromagnetic waves [*Zarka*, 2004]. For example, observations have been made of Auroral Kilometric Radiation (AKR) at Earth, Hectometric Radiation at Jupiter, and Saturn Kilometric Radiation at Saturn. At Earth, AKR is excited from 30 to 800 kHz by precipitating electrons with keV energy in the auroral acceleration region, via the Cyclotron Maser Instability (CMI) [*Wu and Lee*, 1979]. In the CMI process, radio emission is excited via cyclotron resonance with energetic auroral electrons at frequencies close to the local electron cyclotron frequency $f_c = qB/(2\pi m)$ where q is the electron charge, B is the background magnetic field strength, and m is

[1]Institute of Space and Astronautical Science, Japan Aerospace Exploration Agency, Sagamihara, Japan.
[2]LESIA-Observatoire de Paris, CNRS, UPMC University Paris 6, Meudon, France.
[3]University of Leicester, Leicester, UK.
[4]Planetary Plasma and Atmospheric Research Center, Tohoku University, Sendai, Japan.
[5]Solar-Terrestrial Environment Laboratory, Nagoya University, Nagoya, Japan.
[6]Planetary Atmosphere Physics Laboratory, Tohoku University, Sendai, Japan.

Corresponding author: T. Kimura, Institute of Space and Astronautical Science, Japan Aerospace Exploration Agency, 3-1-1 Yoshinodai, Chuo-ku, Sagamihara, Kanagawa 252-5210, Japan. (kimura@stp.isas.jaxa.jp)

2169-9380/13/10.1002/2013JA018833

the electron mass [*Le Quéau and Louarn*, 1989]. Long-term variations in the terrestrial auroral current system have been investigated by several previous studies based on observations of AKR [e.g., *Kumamoto and Oya*, 1998; *Green et al.*, 2004; *Morioka et al.*, 2012]. These studies indicated seasonal variations of the AKR flux densities and spectra, which are suggestive of seasonal variabilities in the auroral acceleration region and associated field-aligned currents. *Kumamoto and Oya* [1998] investigated the meridional distribution of the AKR flux density in winter and summer and found that the flux density is larger in the winter polar hemisphere than the summer hemisphere. Spectral spread and power flux density in the summer and winter hemispheres were investigated for solar maximum and minimum phases by *Green et al.* [2004]. It was clearly demonstrated that AKR spectra are more intense with broader spread in frequency in a darker hemisphere, e.g., AKR spectra are the broadest and most intense in the winter hemisphere during the solar minimum. *Morioka et al.* [2012] continuously monitored the intensity and height distribution of the auroral acceleration region using the AKR spectra as remote proxies over two terrestrial years. They found that the flux density is larger and the acceleration region expansion is higher around the equinox than the solstice while the bottom boundary and peak flux altitude were higher during the summer solstice. They pointed out that there are seasonal variations in the auroral acceleration region driven by two effects: (i) the southward magnetic field effect in the interplanetary magnetic field (IMF) associated with the Russell-McPherron effect [*Russell and McPherron*, 1973] and (ii) the vertical profile of the polar ionospheric plasma. The Russell-McPherron effect is a geometric controlling factor for magnetospheric activities, which determines whether southward IMF is geo-effective or not depending on the season and IMF sector polarity. The intensities and topside altitudes of the acceleration region were found to be positively correlated with the temperature in the plasma sheet with the maxima at the equinoxes. They suggested that in accordance with the Russell-McPherron effect, the electrons are heated when the magnetosphere may be activated by a fluctuative southward component B_z in the IMF. It was also demonstrated that the lowest altitudes of AKR sources and the altitudes of the peak intensities are correlated with the scale height of the polar ionospheric plasma. The latter effect was interpreted as being driven by the solar extreme ultraviolet (EUV) fluxes with maxima around the solstices because of Earth's axial tilt of 23.4°. A north-south asymmetry was also reported in the time difference between northern and southern AKR breakup during the substorm onset [*Morioka et al.*, 2011]. The primary breakup of the AKR during substorms occurred as a "one-sided" breakup in the Northern (summer) Hemisphere without the southern (winter) breakup, followed by a secondary simultaneous breakup in the Northern and Southern hemispheres ∼ 10 min later. The authors interpreted this time difference as the fact that auroral breakup occurs in each hemisphere independently.

[3] Similarly to the AKR excitation process, SKR is excited from 3 to 1200 kHz by energetic (keV) electrons on auroral field lines via the CMI process, with anisotropic directivities in electron phase space density. Based on in situ plasma measurements, remote radio observations, and ultraviolet (UV) auroral imaging, it has been demonstrated that the SKR source region is embedded in a layer of upward current [*Lamy et al.*, 2010] along the field lines connected to the main UV auroral oval [*Lamy et al.*, 2009]. Recently, the long-term variations of Saturn's magnetospheric periodicities have been reported from observations by the Cassini spacecraft over a quarter of 1 kronian year (i.e., 1 kronian year = 29.5 terrestrial years) from 2004 to present (2013). The periodicities of SKR near ∼ 10.7 h were found to be modulated over several years [*Gurnett et al.*, 2009, 2010; *Lamy*, 2011]. These radio emissions indicated a north-south asymmetry with dual, variable periodicities of ∼ 10.8 h for the southern source and ∼ 10.6 h for the northern source during the southern midsummer, which approached each other toward the equinox (August 2009). *Gurnett et al.* [2009, 2010] proposed that these long-term variations are driven by seasonal variations of the ionospheric conductances and not so much zonal winds, which are controlled by the seasonally variable solar UV flux due to the large tilt of Saturn's rotational magnetic axis at 26.7° from the perpendicular to the ecliptic. It should be noted that these long-term variations and north-south asymmetry were also found in the periodicity of the magnetic perturbation fields associated with the magnetosphere-ionosphere (M-I) coupling current system [e.g., *Provan et al.*, 2011; *Andrews et al.*, 2010a, 2010b, 2011, 2012]. These radio and magnetic signatures imply a dynamic M-I coupling process around Saturn's rotational period with a north-south asymmetry depending on season. However, they have not yet been explained self-consistently by only the seasonal solar EUV effects. We should further investigate the seasonal EUV effect based on magnetospheric observables comparing between the Northern and Southern Hemispheres.

[4] It has been indicated by many previous studies that the flux density and periodicity of SKR are strongly correlated with the solar wind on timescales less than the solar rotation (∼ 26 days). The solar wind dynamic pressure is well known to control the SKR intensity [e.g., *Desch and Rucker*, 1983; *Rucker et al.*, 2008; *Badman et al.*, 2008; *Clarke et al.*, 2009; *Taubenschuss et al.*, 2006], while the solar wind velocity has been shown to be well correlated to the short-term variations of the SKR period [*Cecconi and Zarka*, 2005a; *Zarka et al.*, 2007]. It is notable that the solar wind also varies on timescales longer than a solar rotation. During the declining phase of solar cycle 23, *Tokumaru et al.* [2012] indicated a gradual decrease of the solar wind density for the low-velocity solar wind based on the Interplanetary scintillation observations made with the 327 MHz multistation system from 1997 to 2009. *Kataoka and Miyoshi* [2010] indicated that IMF is quite different between 1997 and 2009, which originated from extremely weak open magnetic fields of the Sun [*Wang et al.*, 2009]. We expect this long-term variability of the solar wind to affect the M-I coupling process at Saturn up to solar cycle timescales (11 years).

[5] In this study, variations on timescales shorter than a solar rotation are referred to as "short-term" variations. Those on timescales longer than a few tens of days to 11 years (solar activity) or to a few tens of years (Saturn's orbital period) are referred to as "long-term" variations. From these, Saturn's M-I coupling process is expected to be affected by the solar EUV over a planetary year and by solar wind and solar EUV variations over the solar cycle. This study focuses on the long-term variations in the source

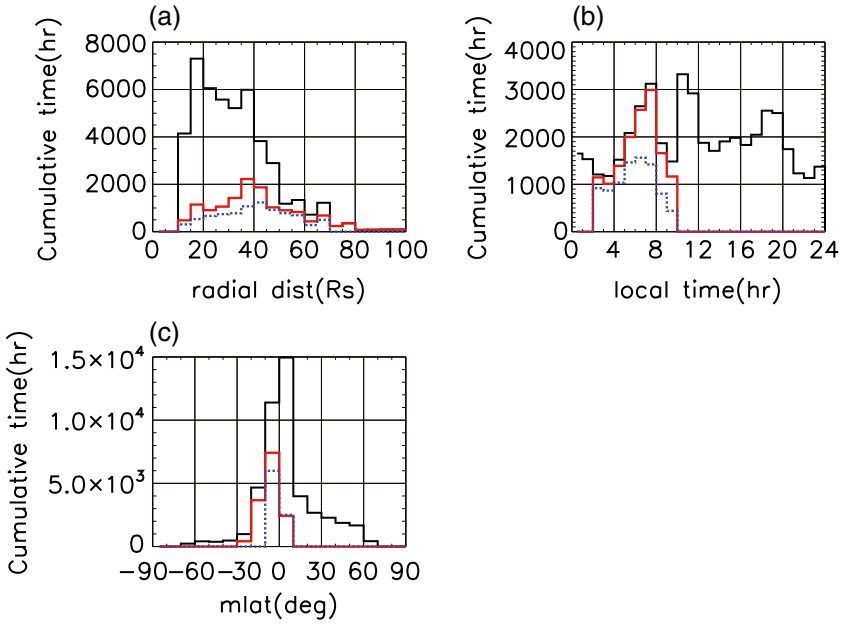

Figure 1. Distribution of cumulative time of RPWS observation in the present analysis period (from DOY 001 2004 to DOY 193 2010). Black solid lines indicate the cumulative time with respect to the (a) radial distance, (b) local time, and (c) latitude of the spacecraft. Red solid lines indicate the cumulative time selected for statistics of the southern SKR (see selection criteria in section 4.2). Blue dotted lines indicate the cumulative time selected for the northern SKR.

region of SKR by removing the short-term variations to identify any seasonal effects on the M-I coupling process at Saturn by comparing SKR with fluctuations of the solar wind and of the solar EUV flux. It should be noted that shadowing by Saturn's rings intensifies darkness during the respective hemisphere's winter especially near the solstice. This effect keeps in phase with the seasonal EUV flux variations. Therefore, the correlation between the solar EUV flux and SKR investigated in this study should also be affected by the ring-shadowing effect. The variation in the intensity and height distribution of the SKR source location was deduced from spectra by the Cassini Radio and Plasma Wave Science experiment (RPWS) [*Gurnett et al.*, 2004]. Finally, we discuss the long-term variations by comparing them with the solar wind parameters, solar EUV flux, and the properties of the Earth's M-I coupling system.

2. Data Set

2.1. SKR Spectra Data Set

[6] We analyzed the spectral densities and polarization of electric fields measured by the RPWS high-frequency receiver (HFR) based on its goniopolarimetric capabilities [*Cecconi and Zarka*, 2005b]. The data set used for this study consists of processed dynamic spectra of SKR flux density in units of W/m^2/Hz normalized to 1 astronomical unit (AU) and its circular polarization, as described in *Lamy et al.* [2008a] (hereafter referred to as L08), whose characteristics are the following. The data cover a frequency range from 3.5 to 1500 kHz with 24 log-spaced channels at 3.5–325 kHz (i.e., δ f/f $\sim$ 20 %) and 24 linearly spaced channels at 325–1500 kHz (i.e., δf = 50 kHz). Interferences in the spectral data are removed based on the method proposed by L08. The data have a time resolution of 10.7 h for seasonal variation analyses in sections 4.2 and 4.3 to remove the periodic variations near the rotational period [e.g., *Gurnett et al.*, 2010]. The data value at a specific sampling time is computed from the median of the raw data (3 min resolution) in a window of $\pm$ 5.35 h centered at the sampling time. The dependence of SKR spectral spread on the spacecraft ephemeris is investigated in section 4.1. The time resolution used to explore the ephemeris dependence is 1 h to highly resolve the spacecraft ephemeris which changes rapidly on timescales shorter than one planetary rotation period near its perikrone. The power flux densities with signal-to-noise ratio greater than 10 dB and magnitude of circular polarization degree |V| greater than 0.2 were retained. The analysis period spans over 6.53 years from the day of year (DOY) 001 2004 to DOY 193 2010. This interval was chosen to match the period of time over which the southern and northern SKR phase systems of [*Lamy*, 2011] are defined. The black solid line in Figure 1 indicates the distribution of cumulative time of RPWS data with respect to the ephemeris of the spacecraft. In the period of analysis, the observations were frequently performed in the southern off-equatorial region (latitudes in the range from –20° to 0°) at distances from 10 to 50 R_s in the dawn sector.

2.2. Solar Wind and Solar EUV Data Set

[7] The solar wind parameters at Saturn's orbit were estimated from the Operating Missions as a Node on the Internet (OMNI) data (http://omniweb.gsfc.nasa.gov) observed around Earth's orbit using a one-dimensional magnetohydrodynamical (MHD) simulation developed by *Tao et al.* [2005]. The proton density, radial velocity, and proton dynamic pressure from the MHD simulation were used for the correlation analysis with the SKR spectral features. The

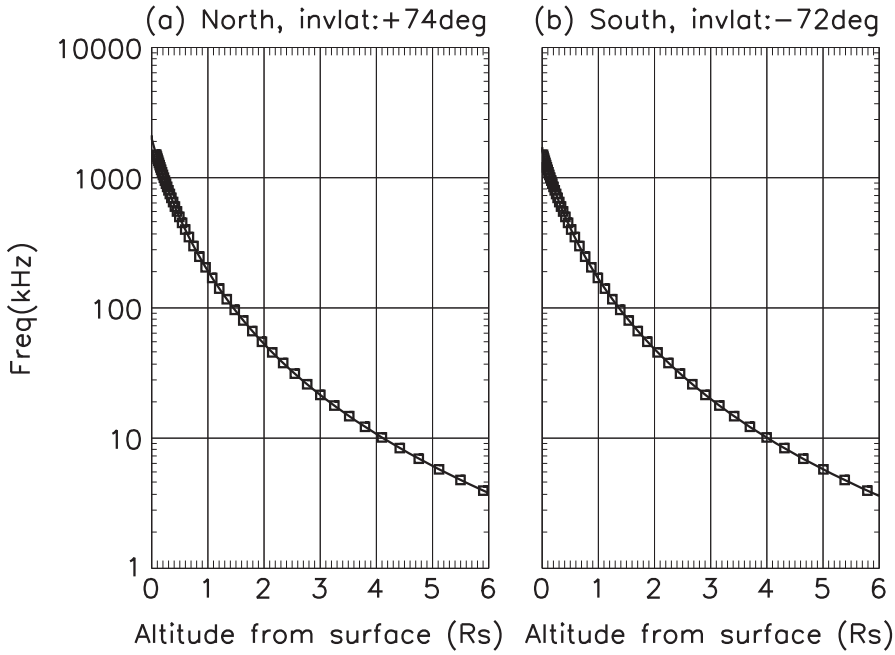

Figure 2. Profiles of the local cyclotron frequency along auroral field lines in the (a) Northern and (b) Southern Hemispheres as functions of altitude from Saturn's surface. Solid lines show the local cyclotron frequency along a magnetic field line with the invariant latitude of +74° (Figure 2a) and –72° (Figure 2b) derived from the internal magnetic field model by *Dougherty et al.* [2005]. Squares along the solid lines indicate locations where the local cyclotron frequency is equivalent to the central frequency at each receiver channel of RPWS/HFR.

time resolution was degraded to that of the SKR data set (i.e., 10.7 h). Based on the solar wind observations by the Ulysses spacecraft at 5.2 AU from Sun, *Tao et al.* [2005] estimated the arrival prediction error of this MHD simulation is at most 2 days for an Earth-Sun-Observer angle less than 60°. We expect the same magnitude of prediction error (but possibly twice larger than the error at Jupiter's orbit) at Saturn's orbit, which is negligible for the correlation analysis of the long-term variations. The solar EUV flux data at 0.1–50 nm are from the database of the Solar Extreme Ultraviolet Monitor (SEM) experiment on the Charge, Element, and Isotope Analysis System (CELIAS) of the Solar and Heliospheric Observatory (SOHO) spacecraft [*Hovestadt et al.*, 1989].

3. Assumptions

[8] The height distribution of the SKR source location was deduced from the SKR spectra with reference to the terrestrial studies by *Morioka et al.* [2008, 2009, 2010, 2011, 2012]. Referring to the validations by previous studies based on remote and in situ measurements in the SKR sources [*Cecconi et al.*, 2009; *Lamy et al.*, 2008a; *Lamy et al.*, 2010, 2011; *Mutel et al.*, 2010; *Menietti et al.*, 2011], we assumed the SKR emissions are predominately right-handed extraordinary (R-X) mode waves excited via the CMI process [*Wu and Lee*, 1979]. The R-X mode waves are right-handed circularly polarized with respect to the background magnetic field. The emission frequency of the SKR spectra can be converted to the corresponding source altitude where the spectral frequency should be equivalent to the local f_c. This is justified by the in situ measurements in the SKR source region [*Lamy et al.*, 2010] which showed the difference between the SKR emission frequency, and the local electron cyclotron frequency has been estimated to be less than 3%. For the frequency-altitude conversion, the magnetic field line was traced from the footprint of the auroral field line at Saturn's surface to the height of the SKR source region.

[9] The internal magnetic field modeled by *Dougherty et al.* [2005] was adopted for the field line tracing. The invariant latitude of the auroral field line was set to be +74° for the northern auroral field line and –72° for the south referring to the imaging results of the auroral main oval [*Badman et al.*, 2006, 2011a; *Lamy et al.*, 2009; *Nichols et al.*, 2009]. Figure 2 indicates profiles of the local cyclotron frequency along the traced auroral field lines in the Northern and Southern hemispheres. The squares in Figure 2 correspond to locations where the local cyclotron frequency is equivalent to the central frequency of each receiver channel of RPWS/HFR. The frequency channels of HFR cover a corresponding altitudinal range from ∼0 R_s to 6 R_s. The northern profile is shifted upward relative to the south because of the magnetic dipole offset of 0.037 R_s.

[10] The sign of circular polarization then provides a simple way to discriminate between southern (left-handed polarized, LH) and northern (right-handed polarized, RH) emissions. Near the equatorial region, the northern component has the right-handed (RH) circular polarization with respect to the k vector, while the southern component has the left-handed (LH) polarization, where the k vector is the wave vector (see *Lamy* [2011] for details). This analysis method enables us to measure the activities in the northern and southern auroral regions simultaneously by the remote sensing of SKR.

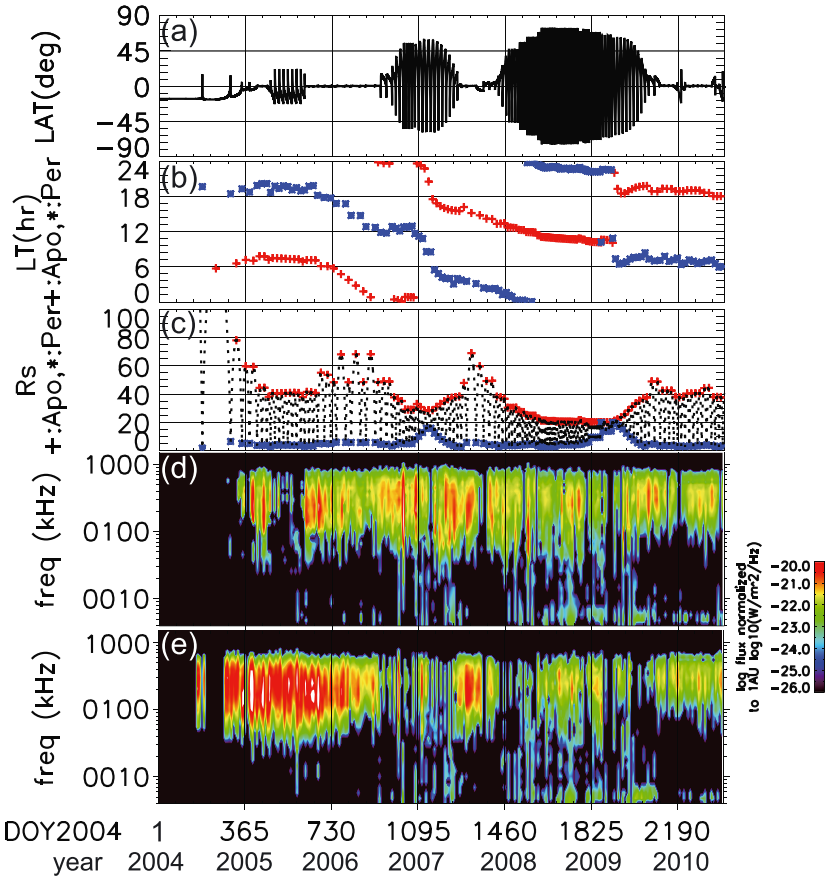

Figure 3. Cassini's ephemeris and frequency-time diagrams of SKR observed by RPWS from DOY 001 2004 to DOY 193 2010. The horizontal axis shows the day of year 2004 with decimal year. (a) Planetographic latitude (degrees), (b) local time (h) of apokrone (red "+") and perikrone (blue "*"), and (c) radial distance (R_s) from Saturn (dotted line) of Cassini. (d) SKR with the right-handed circular polarization corresponding to the northern polar source region. (e) SKR with the left-handed circular polarization corresponding to the southern source region. Color indicates the flux density normalized to 1 AU from Saturn. The vertical axis shows the frequency in kHz.

[11] We note, however, that recent analysis of in situ measurements within an SKR source region did not reveal any Earth-like density cavity (expected from the presence of parallel electric fields) at the temporal resolution of the Cassini Plasma Spectrometer (CAPS) Electron Spectrometer, and underlined that Saturn's auroral regions were naturally sufficiently depleted in cold plasma to drive CMI emission [*Lamy et al.*, 2010; *Schippers et al.*, 2011; *Kurth et al.*, 2011]. As a result, there is no proof yet that the distribution of SKR sources directly probes, as at Earth, the acceleration region.

4. Analysis Result

4.1. Update of Average Properties

[12] As a result of the strong SKR anisotropy, the observed radio signal varies as a function of Cassini's ephemeris (and particularly local time (LT) and latitude, as shown by L08). Figure 3 indicates Cassini's ephemeris and the frequency-time diagram for the interval DOY 001 2004 to 193 2010. SKR both from the northern and southern polar source regions were measured at all Cassini's ephemeris, subsequently showing the ephemeris dependence. To correct for the subsequent bias introduced to our data set, we selected radio data from the spacecraft locations where the SKR spectral shapes are relatively constant (see section 4.2 for the obtained selection criteria). These dependences have already been investigated in the early mission phase by L08 over a few years (2.75 years from DOY 181 2004 to DOY 90 2007). The reanalysis of the dependences has been done in this study over an extended data set.

[13] Figure 4 shows the dependence of median spectra for the northern and southern SKR with the latitude of the spacecraft. The horizontal range is restricted to ± 70° because the bulk of the detected data points was concentrated in that latitudinal range in this period. As already shown by L08, this indicates the latitudinal dependence of observing both SKR above 30 kHz and the narrowband emissions below 30 kHz. The narrowband emissions are suggested to be excited at two frequency bands at 5 and 20 kHz around the plasma torus [*Ye et al.*, 2009; *Wang et al.*, 2010]. They are specifically evident at latitudes below –30° for RH polarized waves and above +40° for LH polarized waves. This characteristic is still observed even when we include both the early and equinox mission phases. From Figure 4a, one can

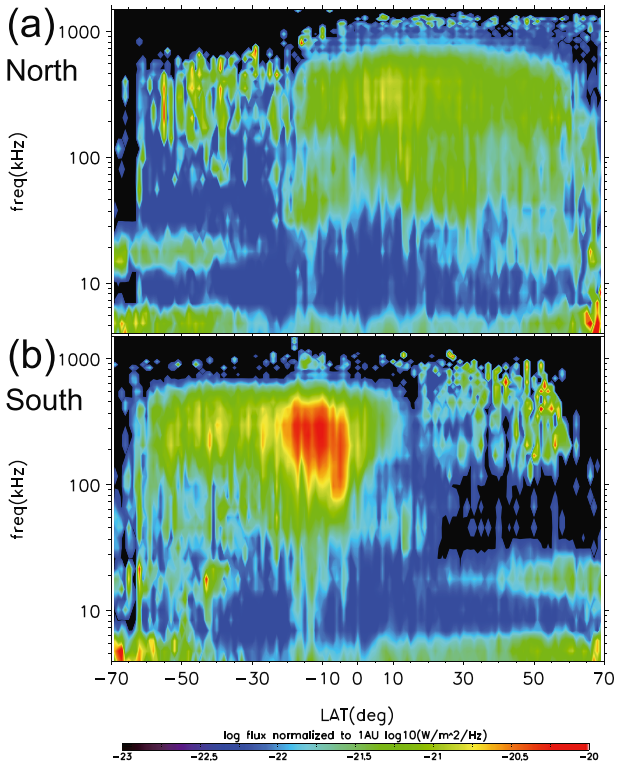

Figure 4. Latitude-frequency diagram showing the dependence of SKR spectra on the latitude of the spacecraft. The analysis period spans from DOY 001 2004 to DOY 193 2010. The horizontal and vertical axes show the latitude of Cassini (degrees) and spectral frequency (kHz), respectively. Colors indicate the flux densities ($W/m^2/Hz$) normalized to the distance of 1 AU from Saturn.

see the SKR from the northern polar region was observed with large flux densities in a wide latitudinal range of the Northern Hemisphere (from –20° up to +70°). The strong southern SKR in Figure 4b was also observed in a wide range of the Southern Hemisphere (–60° to +10°). In the Northern or Southern Hemisphere, the spectral shapes are more dependent on the spacecraft latitude at high latitudes or at the opposite hemisphere than the equatorial region, e.g., spectral spreads of the northern RH SKR rapidly vary from +40° to +70° and –30° to –10°. If the data are successfully selected in the equatorial region (e.g., –5° to +30° for north and –30° to +5° for south), we extract the long-term variations suppressing the apparent variations in the spectral shapes, depending on the spacecraft ephemeris. Another notable characteristic is the north-south asymmetry in the flux density. The maximum flux density at 200–300 kHz is ∼–203 dB in the southern off-equatorial region, which is ∼7 dB higher than the northern off-equatorial flux (∼–210 dB). It should also be noted that there is northern (RH) SKR detected at high southern latitudes and southern SKR (LH) detected at high northern latitudes with a "speckled" appearance in Figure 4. The RH-speckled SKR appears from 60 kHz to 700 kHz between –60° and –20° and LH-speckled SKR from 150 kHz to 900 kHz between +20° and +60°. These components were not reported in L08.

[14] Figure 5 shows the local time dependence of northern and southern SKR spectra in the same format as Figure 4 but as a function of local time. L08 first provided this LT dependence by convolving the northern and southern components during the solstice phase. This study explicitly separated these components based on the polarization measurements. The largest flux densities are observed in the dawn sector (2–10 h) for both the north and south. It should be noted that these flux densities in this diagram indicate the dependence on the local time of the spacecraft location, not necessarily the SKR source location in the polar auroral region. The source location has been identified directly by direction finding. *Lamy et al.* [2009] found the strongest SKR source above the dawn sector of the southern auroral oval during the early phase of Cassini's mission. Our detection of stronger SKR flux densities when Cassini was at dawn may be indicative that the strongest sources continued to be located in the dawn sector when including both the early and equinox phases. Our statistics newly indicate a similar LT dependence of the spectrum in the southern and northern SKR sources. In addition, southern SKR is clearly more intense than northern SKR at comparable latitudes or LT. The high-frequency limit does not indicate much variability, but the low-frequency limit from 30 kHz at 06 LT to greater than 100 kHz at 20 LT is variable for both hemispheres. This variability in the low-frequency limit seems to be an LT dependence rather than at temporal variation because the LT-frequency diagram for each individual year

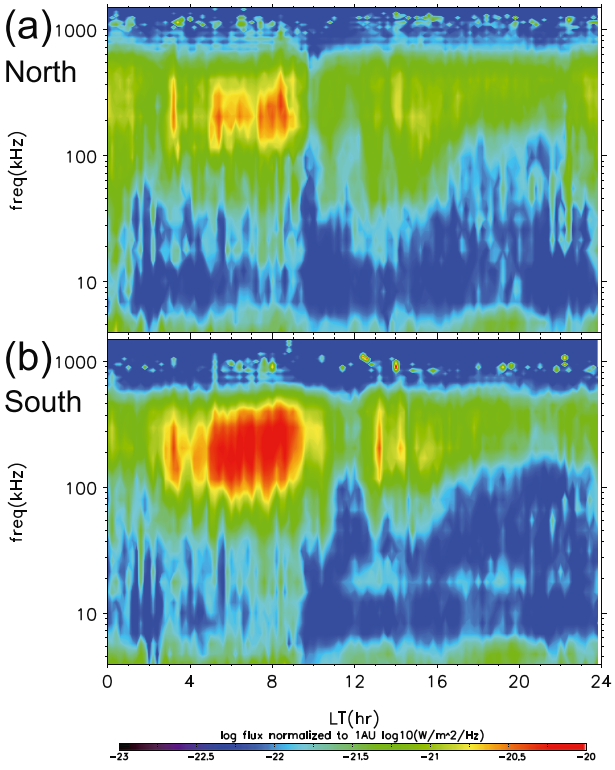

Figure 5. Local time-frequency diagram showing the dependence of SKR spectra on the local time of the spacecraft position, with a similar format to Figure 4, but the horizontal axis shows the local time of Cassini.

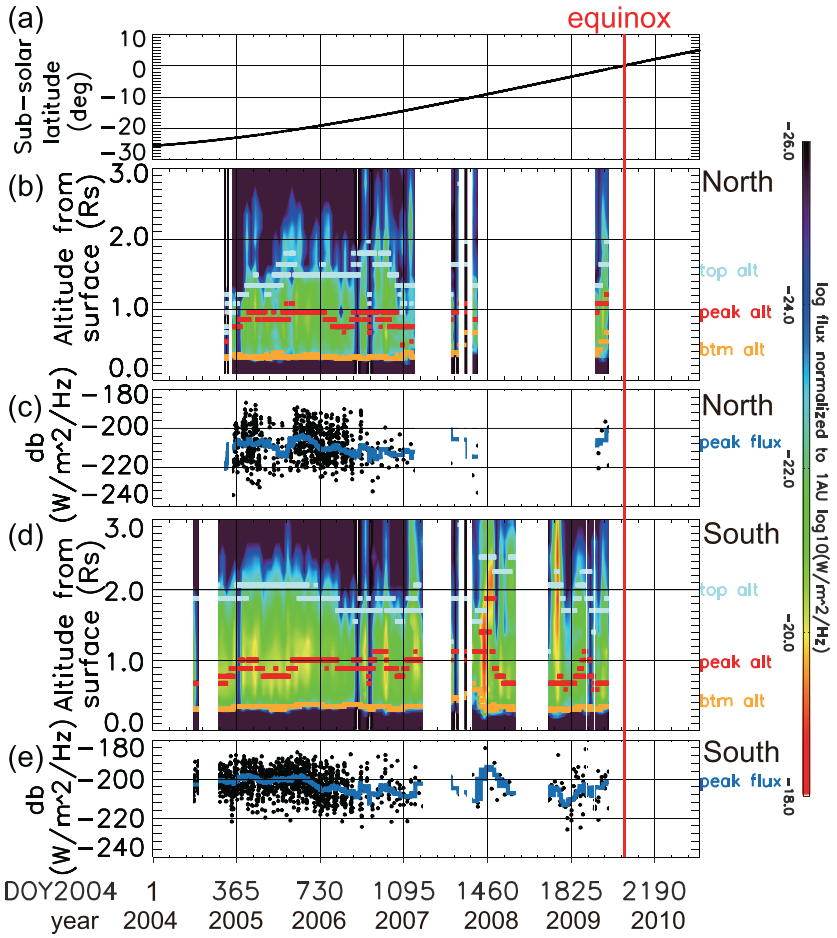

Figure 6. Height distributions of the northern and southern SKR source region as functions of time. The horizontal axis is the day of year (DOY) 2004 corresponding to the period from DOY 1 2004 to DOY 193 2010. (a) Subsolar latitude on Saturn. The red vertical line indicates the equinox in August 2009. (b) Altitude-time diagram indicating the height distribution of the northern SKR source region. The vertical axis shows the source altitude (R_s) from Saturn's surface where the spectral frequency is equivalent to the local electron cyclotron frequency. Colors indicate the flux density (W/m^2/Hz) normalized to a distance of 1 AU from Saturn. The white regions correspond to a lack of observation or a period when the observations did not fulfill the selection criteria described in section 4.2. The overplotted top altitudes (light blue dots), peak flux altitudes (red dots), and bottom altitudes (orange dots) (R_s) were smoothed by a running median with a window of 70 days. The peak flux altitude corresponds to the altitude where the flux density has its maximum value in an altitudinal range from 0 to 2 R_s. The top and bottom altitudes correspond to the FWHM of the peak flux (see section 4.2 for detailed definitions). (c) The peak flux density (W/m^2/Hz) of the northern SKR as a function of time. Black dots represent the peak fluxes detected from each SKR spectra with time resolution of 10.7 h. The blue line shows the smoothed data by a running median with a window of 70 days. (d) Altitude-time diagram and (e) peak flux with the same formats as Figures 6b and 6c but for the southern SKR source.

(not shown) indicates the same broader spread in the dawn sector compared to dusk.

4.2. Height Distribution and Intensity of SKR Source Region

[15] To deduce the long-term M-I coupling process, we estimated the height distribution of the SKR source region from the SKR spectra. Based on the geometric parameter dependence shown in section 4.1, selection criteria for the SKR spectra were defined as follows: (i) the radial distance of the spacecraft spans from 10 to 100 R_s, which easily avoids the equatorial shadow zone at less than 5 R_s (L08) and associated reduction of the signal-to-noise ratio, (ii) the planetographic latitude of the spacecraft is in the range –5° to +30° for the northern SKR and –30° to +5° for the southern SKR (Figure 4), and (iii) the local time of the spacecraft is between 2 and 10 LT to measure the strongest SKR emissions from the observation region of the strongest SKR in the dawn sector as seen in Figure 5. Using these selection criteria, we hope to remove the visibility effect and capture comparable spectral variabilities simultaneously for the north and south near the equatorial region. The criterion (ii) also removes minor L-O mode SKR which was discovered in the hemisphere opposite to the R-X mode SKR by L08.

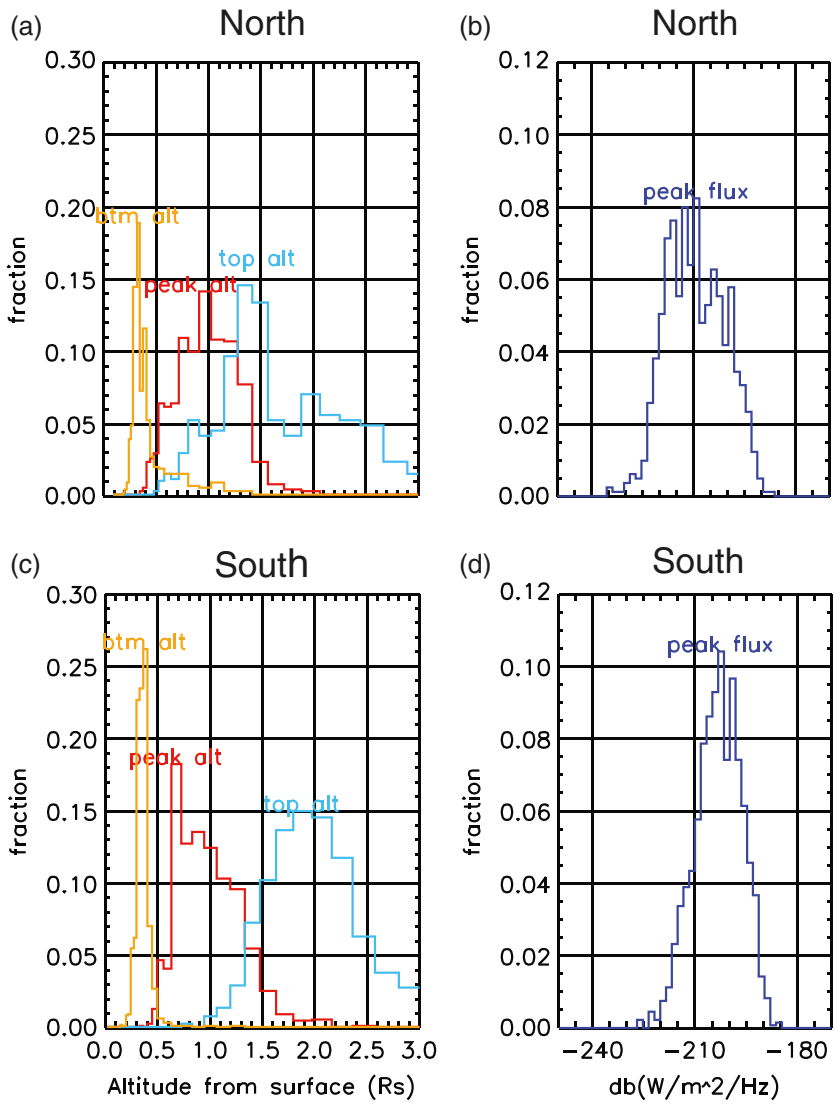

Figure 7. Statistical distribution of the top, peak, and bottom altitudes and the peak flux of the northern and southern SKR source. The parameters for the statistics have a time resolution of 10.7 h without running median. (a) Statistics of the top (light blue), peak (red), and bottom altitudes (orange) for the northern source. The vertical axis is the fraction of the SKR occurrence time with respect to the cumulative operation time at each altitude. The horizontal axis is the altitude (R_s) from the surface. (b) Statistics of the peak flux. The vertical axis is the fraction as described above. The horizontal axis is the flux density (dB). (c and d) Statistics for the southern source with the same formats as Figures 7a and 7b.

The ephemeris distribution when these selection criteria are imposed is shown by the red and blue lines in Figure 1. The cumulative times of the data selected by the criteria were 8507 and 13,930 effective hours for the north and south in the present analysis period, respectively. It should be noted that the northern events are more sparse than the southern ones because intense northern events were observed less frequently due to Cassini's orbital coverage as shown in Figure 1. Based on the detected SKR spectra, the following characteristic altitudes are determined for every spectrum to diagnose the height distribution of the SKR source region: The "peak power flux altitude" is the altitude where the flux density is found to be the maximum in a range less than 2 R_s (larger than $\sim$ 50 kHz), and the "top" and "bottom" altitudes correspond to FWHM of the peak power flux density. The FWHM was defined as the half value of the difference between the peak power flux found below 2 R_s and the noise floor found above 2 R_s. Time series of the SKR spectral features were smoothed by a running median over a time window of 70 days with a time step size of 10.7 h. This smoothing further removes the apparent variation due to visibility at the timescale of the spacecraft orbital motion.

[16] Figure 6 shows the deduced height distribution of the northern and southern SKR source regions. The data in 2004, 2008, and 2010 are sparse because Cassini was located at regions where the detection criteria are not fulfilled. The spacecraft was far from the equatorial region and/or its apokrone was around the dusk sector. One can see

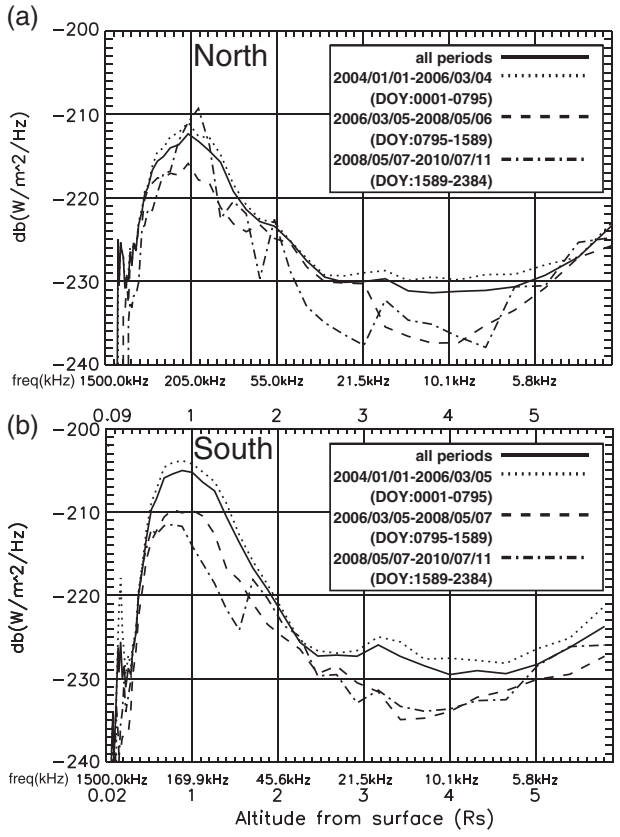

Figure 8. Height distribution of the SKR source deduced from the spectra. (a) Height distribution of the northern SKR source. The vertical axis is the flux density (dB) normalized to a distance of 1 AU. Each line corresponds to a date range indicated in the upper right legend. The median spectrum over the whole analysis period (solid line) is plotted with those from 1 January 2004 to 5 March 2006 (dotted line), from 5 March 2006 to 7 May 2008 (dashed line), and from 7 May 2008 to 11 July 2010 (dash-dotted line). The horizontal axis shows the source altitude (R_s) from the surface with the corresponding cyclotron frequency (kHz). (b) Height distribution of the southern source in the same format as Figure 8a.

the long-term variations in both the northern and southern source regions. The northern and southern source regions expand from the bottom altitudes around 0.3 R_s up to the top altitudes around a few R_s. The peak power flux altitudes are located around 1 R_s for both hemispheres. The bottom altitudes remain approximately constant while the top and peak power flux altitudes are more variable over the analysis period. The southern peak power flux is always larger than the northern peak power flux except for the period around the equinox.

[17] Figure 7 shows the statistical distribution of the top, peak, and bottom altitudes and the peak power flux of the northern and southern SKR over the analysis period. The parameters for the statistics have a time resolution of 10.7 h without running median. It should be noted that Cassini's position fulfilled the selection criteria more frequently during the early phase (midsummer in the Southern Hemisphere) than the last phase (equinox) as shown in Figure 6. Thus, a large proportion of data used in the statistics comes from the early phase. The power flux densities are asymmetric between the northern and southern source regions. The statistical mode of the southern power flux is ~–203 dB, which is 7 dB greater than that of the northern power flux (~ –210 dB). The distributions of the characteristic altitudes are also asymmetric between the northern and southern sources. The altitudinal distributions of the southern top (light blue) altitudes are narrower than those of the north. The statistical modes of the peak power flux altitudes are around 0.8 R_s (~ 250 kHz) for the north and south. The statistical mode of the top altitudes are 1.9 R_s (~ 64 kHz) for the south and 1.3 R_s (~ 124 kHz) for the north. The northern top altitudes are distributed widely, while the southern top altitudes are higher with narrower statistical spreads. In addition, both the northern and southern bottom altitudes (orange) are distributed at the same altitude with narrow spreads. Their statistical modes are ~0.3 R_s (~ 670 kHz and ~ 820 kHz for the south and north) and FWHM is ~ 0.1 R_s both for the south and north.

[18] To further clarify the temporal variation of the altitudinal and power flux distributions, Figure 8 shows the median SKR spectra for the northern and southern components. The height distribution of the SKR source deduced from the spectra is plotted as a function of altitude. Regarding the median spectra over all periods, the southern source region shows a larger power flux density than that of the north. The southern spectral density gradually decreased as the equinox approached. The northern and southern spectral densities became comparable around the equinox (dash-dotted lines). This tendency is evident in the ratio of the southern peak power flux (W/m ^{2}/Hz) to the northern peak power flux (W/m^2/Hz) as a function of time in Figure 9. The south-to-north ratio has a time resolution of 70 days to get simultaneous observations in both hemispheres. The southern-to-northern ratio was as high as 100 during the end of 2004 and then gradually decreased to 2 around the equinox. Figure 10 shows typical examples of *f-t* diagrams for the northern and southern SKR during the midsouthern summer in 2005 (a, b) and just after the equinox in 2009 (c, d). In this figure, we indicate the mixing ratio of the northern and southern SKR power

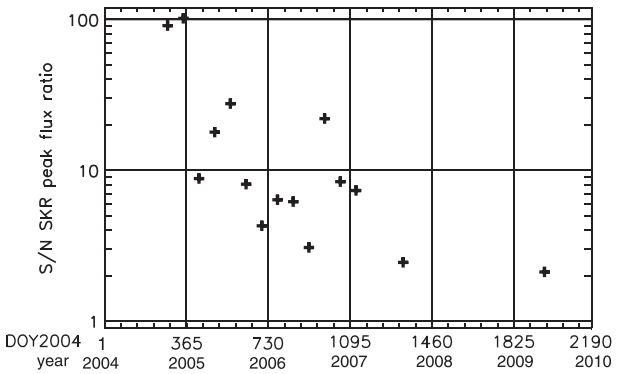

Figure 9. The ratio of the southern peak flux (W/m^2/Hz) to the northern peak flux (W/m^2/Hz) as a function of time with a time resolution of 70 days.

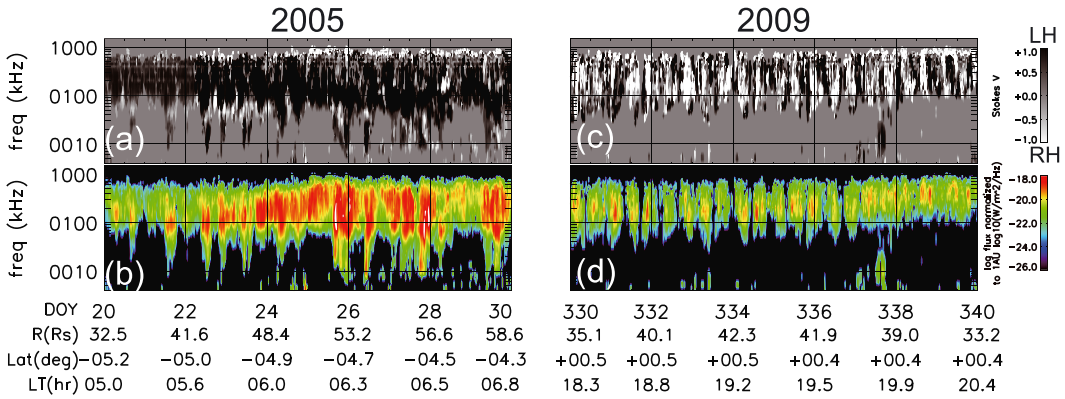

Figure 10. Frequency-time (*f-t*) diagrams indicating Stokes parameter *V* and flux densities for typical examples during the midsouthern summer (2005) and just before the equinox (2009). (a) The *f-t* diagram of Stokes parameter *V* for the SKR observed from DOY 20 to 30 2005. Black indicates a positive value of *V*, corresponding to LH circular polarization, and white indicates a negative value of *V* corresponding to RH circular polarization. (b) The *f-t* diagram of flux density of the northern SKR. Color shows the normalized flux density at 1 AU from Saturn. (c and d) The same diagrams as Figures 10a and 10b but for the SKR from DOY 330 to 340 2009. Ephemeris of Cassini is labeled at the bottom of Figures 10b and 10d.

flux densities in the equatorial region for each year. In 2009, a long sequence of *f-t* diagram could not be acquired over several days in the dawn equatorial region because of Cassini's orbital configuration, so we substituted the data in the dusk equatorial region. It is evident that the peak power flux densities around 100–500 kHz during 2005 were dominated by the LH circular polarization, which is indicative of the southern SKR (panels (a) and (b)). However, the northern (RH) and southern (LH) components were more equally observed around equinox (panels (c) and (d)).

[19] In the present analysis period, the Southern Hemisphere was undergoing midsummer in the early phase and autumn in the last phase. During the early phase, the southern SKR sources were more frequently in the sunlit (summer) region while the northern SKR source region was more frequently in the dark (winter) region. Around the equinox, the southern and northern SKR sources were experiencing a similar amount of a solar flux. Thus, we conclude that the SKR from the summer hemisphere has larger peak power flux than that from the winter hemisphere. This is suggestive of a seasonal effect as has been pointed out based on the periodicity analyses [*Gurnett et al.*, 2009, 2010].

4.3. SKR Response to Long-Term Variations of Solar Wind Parameters and Solar EUV Flux

[20] During the interval under analysis, the solar wind and solar EUV flux varied on the timescale of the solar cycle as shown in Figure 11. It should be noted that this interval overlapped with the declining phase of solar cycle 23. The solar EUV flux in panel (a) gradually decreased over 7 years in this period by a factor ∼2 (from 3.3×10^{10} to 1.7×10^{10} (photons/cm^2/sec)). As evident in the smoothed data in panels (b–d) (blue lines), the dynamic pressure, density, and radial velocity at Earth's orbit vary over several years in this interval with transient enhancements over hundreds of days. These long-term variations are responsible for the same tendency at Saturn (Figures 11e–11g). Originally, the MHD extrapolation of solar wind to Saturn's orbit has an ambiguity in estimating arrival time by a few days as described in section 2.2. This ambiguity is filtered out by this long-term smoothing.

[21] Correlation analyses of the solar wind parameters and solar EUV flux with the SKR source region were performed to investigate the solar wind effects. As in section 4.2, the SKR spectral features were smoothed by a running median over a window of 70 days. The selection criteria are the same as those in section 4.2. The solar wind and EUV flux were also smoothed by the same procedure to remove the short-term variations on timescales less than a few tens of days. Scatterplots for the southern SKR peak power flux, solar wind parameters, and EUV flux are shown in Figure 12 as examples. Correlations between the southern SKR and solar wind are not found in the data set without smoothing (cross-correlation coefficients, CCC= +0.07, +0.09, and +0.10 for the velocity, density, and dynamic pressure, respectively). However, positive correlations were found using the smoothed data (CCC= +0.67, +0.50, and +0.72 for the velocity, density, and dynamic pressure, respectively). These results mean that the larger southern SKR power flux is driven by the disturbed solar wind in the long term: large dynamic pressures and fast flow. Combined with the long-term decrease of the dynamic pressure and radial velocity in Figure 11, we conclude that the southern SKR flux gradually decreased with the solar wind long-term variations on the timescale of the solar activities. The peak power fluxes indicate only weakly positive correlations with the solar EUV flux (CCC= +0.20).

[22] We also compared the ratio of the southern parameters to the northern parameters with the solar wind and EUV flux. The south-to-north ratio has a time resolution of 70 days as indicated in Figure 9. Some examples are indicated in Figure 13. Clear positive correlations are found between the solar EUV flux and the south-to-north ratio of peak power flux and top altitude (CCC= +0.79 and +0.78 for the peak power flux and top altitude, respectively). On the other hand, correlations between the south-to-north ratio

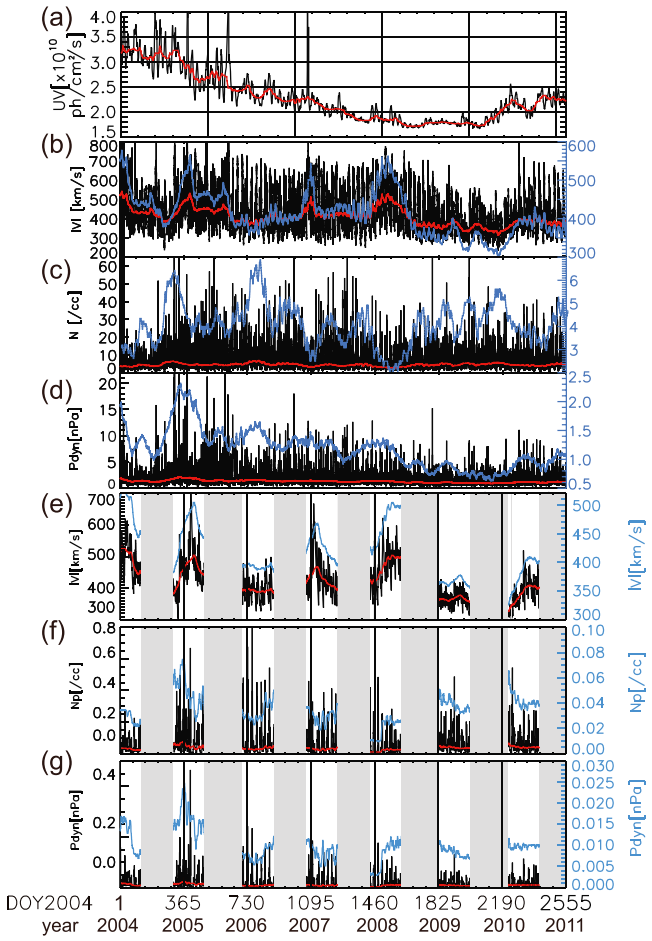

Figure 11. (a) Solar EUV photon flux at 0.1–50 nm (photons/cm^2/s) measured by the SOHO satellite around Earth's orbit from DOY 001 2004 to DOY 001 2011. The black line shows the daily averaged flux as a function of time, and the red line shows the data smoothed by a running median with a window of 70 days. (b–d) Solar wind parameters from OMNI data observed around Earth's orbit, which were used for the initial conditions of the MHD extrapolation to Saturn's orbit. Raw (black), smoothed (red), and rescaled smoothed (blue) data are plotted for the radial velocity (Figure 11b), proton density (Figure 11c), and dynamic pressure (Figure 11d). The blue lines plot the smoothed data equivalent to the red lines but plotted on a smaller scale (blue axes on right-hand side of plot). The smoothed data were computed by the running median with a window of 70 days. (e–g) Solar wind parameters from DOY 001 2004 to DOY 193 2010 at Saturn's orbit, which are extrapolated from Earth's orbit by the MHD simulation. Figures 11e, 11f, and 11g have the same formats as Figures 11b, 11c, and 11d. Gray-shaded regions are periods when the MHD simulation cannot perform a precise estimation of the solar wind arrival time at Saturn due to a phase angle of Earth-Sun-Saturn greater than 60°.

of the bottom altitude and solar EUV flux were not found (CCC= +0.05).

[23] Table 1 summarizes all the correlations of the northern and southern SKR spectral features with the solar wind parameters and solar EUV flux. We compared the parameters of the southern SKR and northern SKR and the ratio of the southern parameters to the northern parameters with the solar wind and EUV flux. It is evident that the peak power fluxes both in the north and south are positively correlated with all the solar wind parameters. In particular, the southern and northern peak power fluxes indicate strongly positive correlations with the dynamic pressure (CCC= +0.72 for both). The southern and northern peak power fluxes indicate much weaker positive correlations with the solar EUV flux (CCC= +0.20, +0.30 for south and north). However, the south-to-north ratio of peak power flux is clearly correlated with the EUV flux (CCC= +0.79). One more notable thing is that the northern and southern bottom altitudes are obviously uncorrelated with all solar wind parameters and solar EUV flux. The top altitudes of southern and northern SKR show negative or positive correlations with some of the solar wind parameters and EUV flux in both the north and south. The northern top altitudes are anticorrelated with all the solar wind parameters(CCC: –0.65 to –0.47). On the other hand, the south-to-north ratio of the top altitudes shows a strongly positive correlation with the EUV flux (CCC= +0.78). The northern and southern peak power flux altitudes show less clear responses to the solar wind and EUV flux relative to the peak power fluxes and top altitudes.

5. Discussion

5.1. Seasonal Variations and North-South Asymmetry

[24] For a long time at the Earth, clear correlations between the power of AKR and the auroral electrojet (AE) index have been pointed out [e.g., *Voots et al.*, 1977; *Morioka et al.*, 2012], meaning that the auroral radio power is correlated with the substorm current system. In this study, we discuss the height spread and power flux density of the SKR source region as proxies of Saturn's auroral activities, expecting them to be analogous to the terrestrial aurora. However, it should be noted that no observation has identified direct relationships between the field-aligned current and SKR flux or the height distribution of the auroral acceleration region and that of the SKR source region. Thus, we must confirm these relations based on in situ measurements in the polar auroral acceleration region associated with SKR parameters in future studies. In addition, the SKR spectra are highly dependent on the position of the spacecraft as shown in Figures 4 and 5. The orbital coverage of Cassini had frequent observations in the Southern Hemisphere dawn sector (Figure 1), which could lead to apparent spectral variations due to the ephemeris dependence, especially at the lower frequencies (Figures 4 and 5). It should be noted that there could still be an observational bias in the statistics of height distribution.

[25] The north-south asymmetry in the power flux ratio (south to north) was found to range from 2 up to 100 (Figure 9). This tendency was also pointed out in the data over 3 years in the early mission period (L08). This asymmetry is indicative of "antiphase" variations in northern

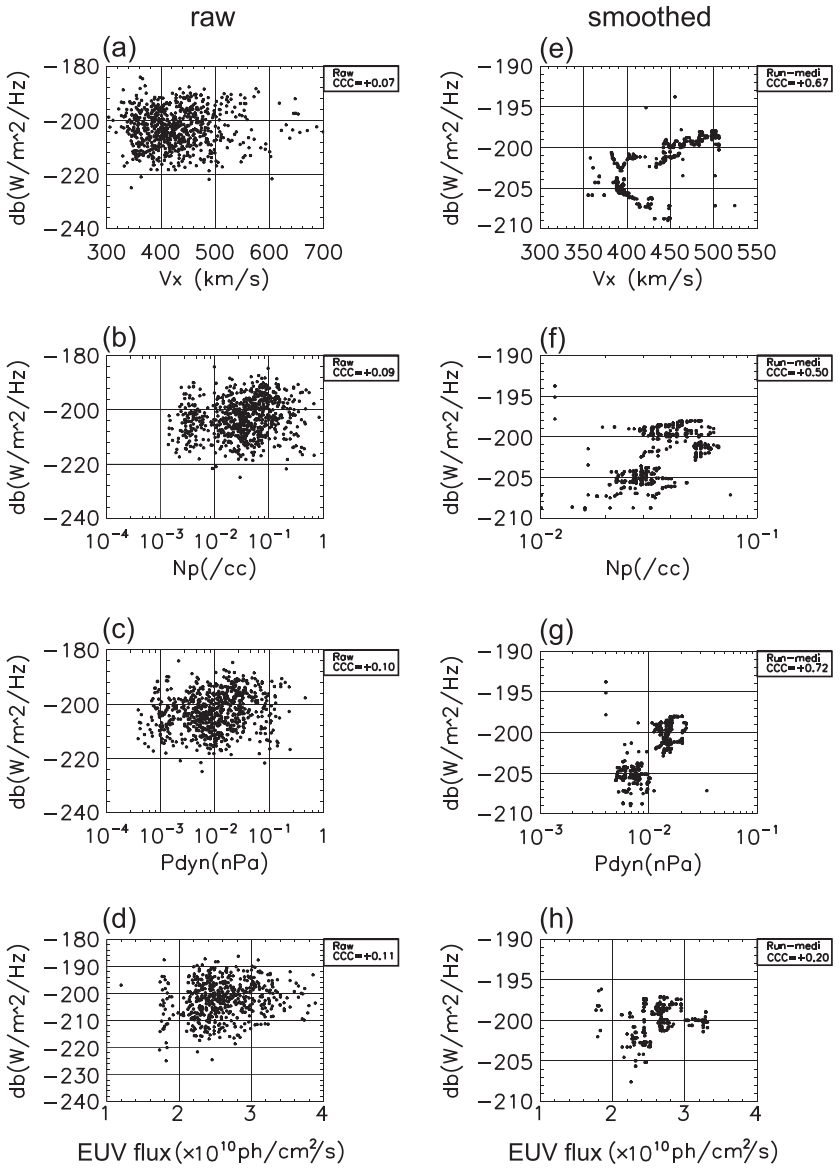

Figure 12. Scatterplots for the southern SKR, solar wind parameters, and solar EUV flux. Scatterplots of data without smoothing (i.e., at 10.7 h resolution) indicates correlations of the southern peak flux versus (a) the radial velocity (km/s), (b) proton density (/cc), (c) dynamic pressure (nPa) of the solar wind, and (d) the solar EUV flux (photons/ cm^2/s). The vertical axes show the peak flux density of the southern SKR (W/m^2/Hz). The cross-correlation coefficients between the southern SKR and solar wind or the southern SKR and solar EUV flux are annotated in the upper right panel for each plot. (e–h) Plots with the same formats as Figures 12a, 12b, 12c, and 12d but for the data smoothed by a running median with a window of 70 days.

and southern SKR in terms of the seasonal effect. In contrast, the positive correlations (CCC= +0.72) are evident for both the northern and southern power fluxes with the dynamic pressure. This result suggests that northern and southern SKR are "inphase" with each other in terms of the solar wind response. The inphase variations are possibly due to the simultaneous response of northern and southern SKR sources by global solar wind compression. The inphase variations are weaker for the south-to-north ratio while the antiphase variations are stronger, as shown by the correlation analysis in Figure 13 and Table 1. Thus, we interpret the clear positive correlations of south-to-north ratios of peak power flux and top altitude with the solar EUV flux (CCC= +0.79, +0.78) as a result of the seasonal variations in the solar illumination at each hemisphere. From these results, we speculate that the auroral activities above the summer polar ionosphere are more intense than those above the winter polar ionosphere, which are probably related to ionospheric modifications in response to the EUV flux. The stronger source region in the south is suggestive of more unstable phase space density of auroral electrons penetrating into the summer polar ionosphere. It should be noted that the solar illumination has the long-term variation of the total EUV flux by a factor 2 as indicated in Figure 11. This could

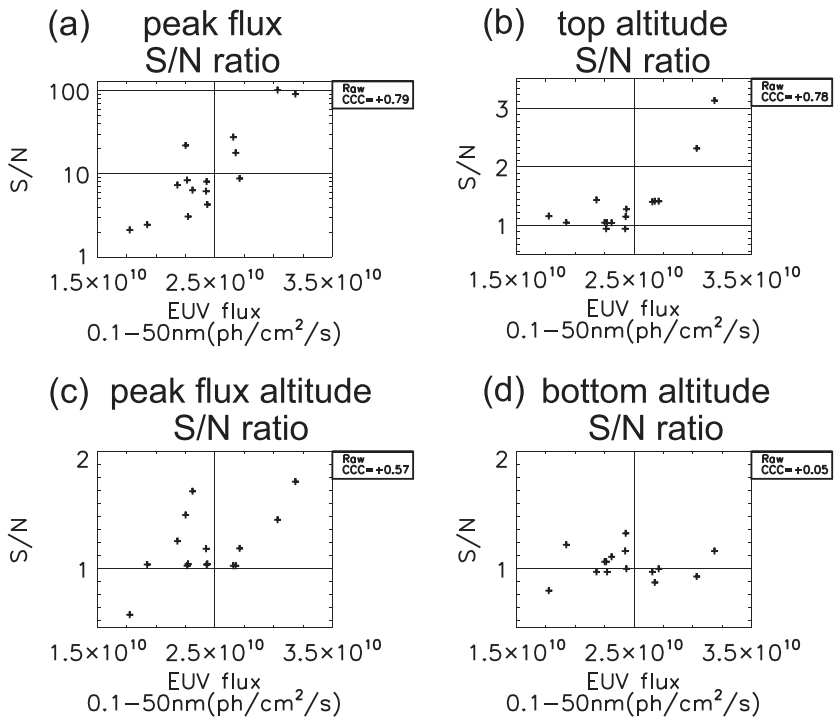

Figure 13. Scatterplots for the ratio of the southern SKR parameters to the northern SKR parameters and solar EUV flux. The time resolution is 70 days. Scatterplots indicate correlations of the EUV flux (photons /cm^2/s) versus the south-to-north ratio of (a) peak flux, (b) top altitude, (c) peak flux altitude, and (d) bottom altitude. The formats are the same as the panels in Figure 12.

affect the polar ionosphere as the second-order effect (see section 5.2 for details).

[26] This is the same conclusion that was reached from the study of the infrared (IR) auroral main oval imaged by Cassini during the southern summer period [*Badman et al.*, 2011b]. *Badman et al.* [2011b] indicated that the southern main auroral oval is more intense by a factor of 1.3 than the north. Consistently, the bulk of SKR is known to be emitted on field lines connected to the main oval [*Lamy et al.*, 2009]. *Badman et al.* [2011b] proposed some candidates for the north-south asymmetric IR aurora: the asymmetries of precipitating electron power, ionospheric conductance, or Joule heating, which are caused by the larger solar EUV flux in the southern ionosphere and consequently responsible for the stronger southern main oval. In both cases of SKR and IR aurora, we would expect the stronger auroral activities above the sunlit polar ionosphere. As Saturn's season passes through the equinox, the southern activities could decrease until the northern SKR becomes stronger than the southern SKR if the polar ionosphere responds linearly. The comparable power flux of the northern and southern SKR around the equinox shown in Figures 8 and 9 also supports the above possibility. We need to investigate the post equinox period with further sufficient data volume to examine the crossover of the northern and southern auroral activities. Unfortunately, the apokrone of Cassini has been in the dusk to dayside after this analysis period to the present (2013), and recently, Cassini is in another high-inclination phase. Thus, the appropriate geometry for this study, i.e., low latitudes in the dawn sector, is not satisfied by the recent orbits. Our approach for the northern summer will be performed in the period when Cassini will revisit the dawn low latitudinal region in the near future.

[27] Based on the statistics of the in situ azimuthal magnetic fields above the nightside polar ionosphere in 2008, *Talboys et al.* [2011] indicated that the field-aligned currents in the north and south are of the same order of magnitude, and their difference does not exceed the observational uncertainty. This result needs to be reconciled with the above north-south asymmetry of the IR aurora and SKR. Possible solutions are that a small amount of events (30 periapsis passes) with large variability in each could not figure out the statistical north-south asymmetric features and/or the investigated local time sectors (nightside sector) had different current flows from the dawn sector in our study. The instantaneous solar wind variations could be a cause for the variability in each event because the CMEs and CIRs largely affect the strength of SKR, suggestive of the short-term variability in the auroral field-aligned currents. The in situ observations in the southern polar magnetosphere by *Bunce et al.* [2010] actually indicated an unusual intensification of the field-aligned currents on day 291 2008. That intensification was accompanied by the contraction of the open field region, hot keV electron populations, and SKR extending toward low frequencies. These signatures were suggested to be triggered by a solar wind compression. Unfortunately, a direct comparison between the solar wind and in situ field-aligned currents has not been achieved because of the observations by one spacecraft in the magne-

Table 1. Summary of Cross-Correlation Coefficients

	Southern SKR[a]			
	Peak Flux	Top Altitude	Peak Flux Altitude	Bottom Altitude
V_x	+0.67	+0.56	+0.15	–0.05
N_p	+0.50	–0.07	–0.42	0.00
P_{dyn}	+0.72	+0.21	–0.26	–0.01
f_{EUV}	+0.20	–0.06	–0.37	–0.02
	Northern SKR[a]			
	Peak Flux	Top Altitude	Peak Flux Altitude	Bottom Altitude
V_x	+0.58	–0.61	+0.14	+0.10
N_p	+0.66	–0.50	–0.03	+0.09
P_{dyn}	+0.72	–0.65	+0.03	+0.08
f_{EUV}	+0.30	–0.47	–0.50	–0.13
	Southern-to-Northern Ratio[b]			
	Peak Flux	Top Altitude	Peak Flux Altitude	Bottom Altitude
V_x	+0.14	+0.17	+0.13	–0.14
N_p	+0.54	+0.34	+0.08	0.00
P_{dyn}	+0.51	+0.38	+0.10	–0.09
f_{EUV}	+0.79	+0.78	+0.57	+0.05

[a]Smoothed over 70 days with 10.7 h resolution.
[b]With 70 days resolution.

tosphere. The long-term analyses for the in situ field-aligned currents are necessary to flatten the short-term variability and extract the seasonal variability of the polar field-aligned currents for the comparison with the remotely detected auroral processes.

[28] This study also indicated that the bottom altitudes of the SKR source (0.3 R_s) are the same in the north and the south. L08 found a systematic extension of the northern spectra toward higher frequencies (by 50 to 100 kHz) than the south above 200 kHz (i.e., below 1 R_s). This corresponds to the expansions of northern bottom altitudes toward low altitudes. In that case, if the iso-contours of local f_c are centered at Saturn, the northern bottom altitudes are lower than the south as measured from Saturn's surface. However, the iso-contour is actually shifted northward from the planet center by the magnetic dipole offset of 0.037 R_s. Thus, the northward shift compensates for the lower expansion of the northern bottom altitudes. The higher-frequency expansions of 50 to 100 kHz are equivalent to downward altitudinal expansions of less than 0.1 R_s around 0.3 R_s. Although both the lower expansions and northward shift are small with respect to the altitudes of interest (i.e., 0.3 R_s), they cancel each other, which is consistent with the determination of the same bottom altitudes at 0.3 R_s in the north and south.

5.2. Variations on the Solar Cycle Timescale

[29] In section 4.3, the smoothed southern and northern peak power fluxes were found to be well correlated with the dynamic pressure during the declining phase of the solar cycle. Even though the northern SKR was found to be less intense and less variable than the southern SKR (Figures 7 and 8), it significantly responds to the dynamic pressure. This correlation straightforwardly suggests that large SKR fluxes are emitted from both the summer and winter hemispheres during solar wind compressions of Saturn's magnetosphere. This is not the first report of the positive correlations between SKR and the solar wind dynamic pressure (or radial velocity), which has long been reported from the short-term observations in the timescale less than the solar rotation (∼ 26 days) [e.g., *Desch and Rucker*, 1983; *Rucker et al.*, 2008]. A gradual decrease of the peak power flux can also be seen in the data during the early mission period from late 2005 to mid-2006 (see Figure 9 of L08). What this study has newly confirmed is that the solar wind responses were evident in both north and south, and they continued into later mission phases through different solar activities.

[30] The long-term variation by the solar wind is an important factor for the long-term variations of SKR in addition to the seasonal variations by the solar EUV. From the scatterplot for the smoothed data in Figures 12e–12h, the dynamic range of the southern peak power flux was found to be ∼ 16 dB (–210 to –194 dB), which leads to the radio energy flux range of a factor ∼40. This dynamic range is significant with respect to the southern-to-northern peak power flux ratio of up to 100 during the midsouthern summer (see Figure 9). If we roughly assume that the peak power flux is seasonally symmetric between the midsummer and midwinter, we can regard this south-north ratio of less than 100 as a typical amplitude of the seasonal variations. Then the amplitude of the solar wind variations are significant with respect to the seasonal variations in this analysis period. This points out a possibility that the solar wind variations on the solar cycle timescale affect the long-term M-I coupling process on top of the baseline of the seasonal variations. The physical process of the intensification of the SKR source

Table 2. Comparisons of Auroral Acceleration Regions at Earth and Saturn for the Long-Term Variations

	AKR at Earth [*Morioka et al.*, 2012]	SKR at Saturn (This Study)
Peak flux		
Relevant factor	IMF B_z[a]	EUV[b] and SW[c]
Top altitude		
Altitude	0.9–1.4 R_e	1.3–1.9 R_s
Relevant factor	IMF B_z[a]	EUV[b]?
Peak flux altitude		
Altitude	0.9 R_e	0.7–0.9 R_s
Relevant factor	EUV[b]	?
Bottom altitude		
Altitude	0.4–0.6 R_e	∼ 0.3 R_s
Relevant factor	EUV[b]	Constant

[a]IMF B_z: effect of north-south component B_z in the Interplanetary Magnetic Field.
[b]EUV: seasonal solar EUV effect.
[c]SW: solar wind compressional effect in the timescale of solar cycle.

region by the solar wind compression has not been established. However, it would be expected that the SKR source is associated with the auroral field-aligned current system driven by the flow shear between the high latitude, antisunward open field line flows, and the subcorotating magnetospheric plasma theoretically proposed by *Cowley et al.* [2004]. In that theory, the field-aligned current system depends on the radial gradient of the angular velocity in the subcorotating plasma. The magnetospheric compression by the solar wind possibly steepens the angular velocity profile of the subcorotating plasma. The auroral field-aligned current and associated SKR are expected to be intensified by the profile change. We speculate this relationship works in the long term.

[31] The EUV flux variation related to the solar activity is possibly another relevant parameter for the long-term variations in the SKR source region. The decreasing total solar EUV flux in this data set possibly emphasizes the decrease of solar illumination in the south and suppresses the increase of solar illumination in the north. As shown in Figure 11, the solar EUV flux was decreasing by a factor ~ 2 due to the solar activities. In the southern polar region, the seasonal solar EUV flux decreases through summer to autumn. This seasonal decrease is inphase with the decrease by the solar activities. On the other hand, the seasonal solar EUV flux increases through winter to spring in the northern polar region. This seasonal increase is in antiphase with the solar activities. The total solar illumination in the north tends to be suppressed by the antiphase variations. Consequently, if we assume a linear response of SKR flux to the input solar EUV flux, the variable southern SKR is expected to dominate over the invariable winter SKR in the south-to-north ratio. It should be noted that in this data set, it is difficult to clearly deconvolve the EUV variations by season and by the solar activity. However, the gradual decrease of the south-to-north ratio of SKR power flux in Figure 9 and good positive correlations with the total EUV flux are consistent with this story.

5.3. Comparison With Earth

[32] As briefly mentioned in the introduction, *Morioka et al.* [2012] thoroughly investigated the long-term variations of Earth's auroral acceleration region based on AKR spectra observed by the Polar spacecraft over 18 months from 1996 to 1997. They demonstrated that the terrestrial auroral acceleration region is controlled by both the seasonal effects of the solar EUV flux and IMF B_z through the Russell-McPherron effect [*Russell and McPherron*, 1973]. The solar EUV illumination causes annual variations of the photoionization rate in the polar ionosphere. One enhancement of the photoionization is caused per terrestrial year in one hemisphere around solstice as expected at Saturn. On the other hand, the Russell-McPherron effect is associated with geo-effective southward IMF, which is determined by the season and IMF sector polarity. At the equinoxes, the IMF B_z in the geocentric solar magnetospheric coordinate should have the largest value if the IMF sector polarity directs the right way, e.g., the IMF is aligned with the magnetic axis direction. Based on the AKR spectral features during the off-breakup phase of substorms, *Morioka et al.* [2012] indicated the correlations of the auroral acceleration region with the magnetospheric and ionospheric parameters: (i) the positive correlation of the peak power flux and top altitudes of AKR source region with plasma sheet temperature and AE index, and (ii) the positive correlations of the peak power flux altitude and bottom altitude with scale height of ionospheric electron density. *Morioka et al.* [2012] interpreted correlation (i) as the B_z effect on the magnetosphere, which drives the plasma sheet heating followed by the intensification of the M-I coupling auroral currents. Correlation (ii) was interpreted as the solar EUV effect on the polar ionosphere, which enhances the scale height of the polar ionospheric plasma, and the plasma cavity of the auroral acceleration region is filled by the ionospheric plasma at the bottom altitudes. *Green et al.* [2004] also investigated the seasonal variations of AKR for each solar activity. They found a stronger AKR flux in the winter hemisphere than in the summer hemisphere and that both winter and summer AKR are more intense during the solar maximum than the solar minimum. They interpreted that AKR activities are decreased by filling of the plasma density cavity due to large solar EUV flux during summer and maximum solar activity.

[33] These features of the terrestrial auroral acceleration region are in completely the opposite sense to the SKR characteristics identified here for Saturn. The results in this study imply that Saturn's auroral acceleration region has variabilities which are essentially different from Earth in the long term. The peak power flux had its largest value during the summer, and the top altitudes were not higher around the equinox than the other periods. This tendency indicates that the IMF B_z effect at Saturn is insignificant or not inphase with Earth even though it is well expected by analogy with Earth based on the larger tilt of rotational axis at Saturn (26.7°) than that at Earth (23.4°). The different dependence on the IMF B_z between Earth and Saturn could be due to the difference of the solar wind polarity at each orbit, plasma beta conditions around the magnetopause as suggested by *Masters et al.* [2012], or other unknown factors. The absence of the IMF B_z effect is in agreement with earlier observations that Saturn's magnetosphere and aurorae are more effectively controlled by the solar wind dynamic pressure than the IMF polarity [*Crary et al.*, 2005]. The bottom altitudes of the SKR source region were not found to be correlated with the solar wind or EUV flux. This suggests that the bottom altitude of the SKR source region is not controlled by the variation of the polar ionospheric scale height, i.e., there is no significant depletion and repletion of the auroral plasma cavity. Nondetection of the plasma cavity in Saturn's auroral region [*Lamy et al.*, 2010; *Schippers et al.*, 2011] is consistent with these terrestrial cases. The absence of the plasma cavity could be a major difference between Earth and Saturn. Table 2 summarizes the comparisons of the auroral acceleration regions at Earth and Saturn deduced from the auroral radio emissions. The height distribution of the auroral acceleration region at each planet is normalized by the planetary radii.

[34] We found that Saturn's top altitudes are somehow strongly anticorrelated with all the solar wind parameters and EUV flux only in the Northern Hemisphere. This anticorrelation indicates that the top altitudes in the winter hemisphere decreased during the solar wind compression period and/or high-solar activities. There is no physical candidate for the explanation of these characteristics even if we refer to AKR characteristics at Earth. We should further

investigate the altitudinal expansion of the SKR sources, consistently separating the dark and sunlit hemispheres.

6. Summary

[35] In this study, the long-term variations of the SKR source region were investigated based on the SKR spectra during the southern summer (from DOY 001 2004 to DOY 193 2010) and compared with the solar wind and solar EUV flux on the timescale of solar activity. It was found that on average, the southern SKR peak spectral density was up to 100 times greater than that of the north, and the altitude of the flux maxima was $\sim 0.8\ R_s$ for the north and south. The southern and northern spectral densities became comparable with each other at the equinox. These results suggest the relatively stronger auroral activities during the summer than the winter. A long-term correlation analysis was performed for the SKR spectral features, solar EUV flux, and solar wind parameters extrapolated from Earth's orbit by an MHD simulation. The SKR spectral features, solar EUV flux, and solar wind parameters were smoothed by a running median with a time window of 70 days. The solar EUV flux and some solar wind parameters were gradually decreasing during the declining phase of the solar activities. Clear positive correlations between the solar wind dynamic pressure and peak flux density were found in both of the Southern and Northern Hemispheres (CCC= +0.72). They imply that solar wind compressions on timescales of the solar cycle control the northern and southern auroral activities. It was also confirmed that the ratio of southern SKR parameters (peak flux and top altitude) to northern SKR parameters is positively correlated with the solar EUV flux (CCC= +0.79, +0.78). This result strongly supports the seasonal EUV effect on the SKR source region. The comparison with Earth's auroral acceleration region suggested that the IMF B_z effect and scale height effect of the polar ionospheric plasma are insignificant to Saturn's auroral radio source, which is rather attributed to the seasonal EUV and solar wind pressure in the long term.

[36] **Acknowledgments.** This research was supported by a grant-in-aid for Scientific Research from the Japan Society for the Promotion of Science (JSPS). French coauthors were supported by CNRS (Centre National de la Recherche Scientifique), Observatoire de Paris, and CNES (Centre National d'Etudes Spatiales). S.V.B. was supported for part of this study by a Royal Astronomical Society Research Fellowship. The OMNI data were obtained from the GSFC/SPDF OMNIWeb interface at http://omniweb.gsfc.nasa.gov. Especially, the authors acknowledge all the PIs of IMP-8, WIND, ACE for the recent contributions to OMNI. The authors also acknowledge the team of the CELIAS/SEM experiment on the SOHO spacecraft.

[37] Philippa Browning thanks the reviewers for their assistance in evaluating this paper.

References

Andrews, D. J., S. W. H. Cowley, M. K. Dougherty, and G. Provan (2010a), Magnetic field oscillations near the planetary period in Saturn's equatorial magnetosphere: Variation of amplitude and phase with radial distance and local time, *J. Geophys. Res.*, *115*, A04212, doi:10.1029/2009JA014729.

Andrews, D. J., A. J. Coates, S. W. H. Cowley, M. K. Dougherty, L. Lamy, G. Provan, and P. Zarka (2010b), Magnetospheric period oscillations at Saturn: Comparison of equatorial and high latitude magnetic field periods with north and south Saturn kilometric radiation periods, *J. Geophys. Res.*, *115*, A12252, doi:10.1029/2010JA015666.

Andrews, D. J., B. Cecconi, S. W. H. Cowley, M. K. Dougherty, L. Lamy, G. Provan, and P. Zarka (2011), Planetary period oscillations in Saturn's magnetosphere: Evidence in magnetic field phase data for rotational modulation of Saturn kilometric radiation emissions, *J. Geophys. Res.*, *116*, A09206, doi:10.1029/2011JA016636.

Andrews, D. J., S. W. H. Cowley, M. K. Dougherty, L. Lamy, G. Provan, and D. J. Southwood (2012), Planetary period oscillations in Saturn's magnetosphere: Evolution of magnetic oscillation properties from southern summer to post-equinox, *J. Geophys. Res.*, *117*, A04224, doi:10.1029/2011JA017444.

Badman, S. V., et al. (2006), A statistical analysis of the location and width of Saturn's southern auroras, *Ann. Geophys.*, *24*(12), 3533–3545.

Badman, S. V., S. W. H. Cowley, L. Lamy, B. Cecconi, and P. Zarka (2008), Relationship between solar wind corotating interaction regions and the phasing and intensity of Saturn kilometric radiation bursts, *Ann. Geophys.*, *26*, 3641–3651.

Badman, S. V., N. Achilleos, K. H. Baines, R. H. Brown, E. J. Bunce, M. K. Dougherty, H. Melin, J. D. Nichols, and T. Stallard (2011a), Location of Saturn's northern infrared aurora determined from Cassini VIMS images, *Geophys. Res. Lett.*, *38*, L03102, doi:10.1029/2010GL046193.

Badman, S. V., C. Tao, A. Grocott, S. Kasahara, H. Melin, R. H. Brown, K. H. Baines, M. Fujimoto, and T. Stallard (2011b), Cassini VIMS observations of latitudinal and hemispheric variations in Saturn's infrared auroral intensity, *Icarus*, *216*, 367–375, doi:10.1016/j.icarus.2011.09.031.

Bunce, E. J., et al. (2010), Extraordinary field-aligned current signatures in Saturn's high-latitude magnetosphere: Analysis of Cassini data during Revolution 89, *J. Geophys. Res.*, *115*, A10238, doi:10.1029/2010JA015612.

Cecconi, B., and P. Zarka (2005a), Model of a variable radio period for Saturn, *J. Geophys. Res.*, *110*, A12203, doi:10.1029/2005JA011085.

Cecconi, B., and P. Zarka (2005b), Direction finding and antenna calibration through analytical inversion of radio measurements performed using a system of 2 or 3 electric dipole antennas, *Radio Sci.*, *40*, RS3003, doi:10.1029/2004RS003070.

Cecconi, B., L. Lamy, P. Zarka, R. Prangé, W. S. Kurth, and P. Louarn (2009), Goniopolarimetric study of the revolution 29 perikrone using the Cassini Radio and Plasma Wave Science instrument high-frequency radio receiver, *J. Geophys. Res.*, *114*, A03215, doi:10.1029/2008JA013830.

Clarke, J. T., et al. (2009), Response of Jupiter's and Saturn's auroral activity to the solar wind, *J. Geophys. Res.*, *114*, A05210, doi:10.1029/2008JA013694.

Cowley, S. W. H., E. J. Bunce, and J. M. O'Rourke (2004), A simple quantitative model of plasma flows and currents in Saturn's polar ionosphere, *J. Geophys. Res.*, *109*, A05212, doi:10.1029/2003JA010375.

Crary, F. J., et al. (2005), Solar wind dynamic pressure and electric field as the main factors controlling Saturn's aurorae, *Nature*, *433*, 720–722, doi:10.1038/nature03333.

Desch, M. D., and H. O. Rucker (1983), The relationship between Saturn kilometric radiation and the solar wind, *J. Geophys. Res.*, *88*, 8999–9006.

Dougherty, M. K., et al. (2005), Cassini magnetometer observations during Saturn orbit insertion, *Science*, *307*, 1266–1270, doi:10.1126/science.1.106098.

Green, J. L., S. Boardsen, L. Garcia, S. F. Fung, and B. W. Reinisch (2004), Seasonal and solar cycle dynamics of the auroral kilometric radiation source region, *J. Geophys. Res.*, *109*, A05223, doi:10.1029/2003JA010311.

Gurnett, D. A., et al. (2004), The Cassini radio and plasma wave investigation, *Space Sci. Rev.*, *114*, 396–463.

Gurnett, D. A., A. Lecacheux, W. S. Kurth, A. M. Persoon, J. B. Groene, L. Lamy, P. Zarka, and J. F. Carbary (2009), Discovery of a north-south asymmetry in Saturn's radio rotation period, *Geophys. Res. Lett.*, *36*, L16102, doi:10.1029/2009GL039621.

Gurnett, D. A., J. B. Groene, A. M. Persoon, J. D. Menietti, S.-Y. Ye, W. S. Kurth, R. J. MacDowall, and A. Lecacheux (2010), The reversal of the rotational modulation rates of the north and south components of Saturn kilometric radiation near equinox, *Geophys. Res. Lett.*, *37*, L24101, doi:10.1029/2010GL045796.

Hovestadt, D. J., et al. (1989), CELIAS - Charge, Element, and Isotope Analysis System for SOHO, in *The SOHO Mission,* ESA, vol. SP-1104, pp. 69–74.

Kataoka, R., and Y. Miyoshi (2010), Why are relativistic electrons persistently quiet at geosynchronous orbit in 2009?, *Space Weather*, *8*, S08002, doi:10.1029/2010SW000571.

Kumamoto, A., and H. Oya (1998), Asymmetry of occurrence-frequency and intensity of AKR between summer polar region and winter polar region sources, *Geophys. Res. Lett.*, *25*, 2369–2372, doi:10.1029/98GL01715.

Kurth, W. S., et al. (2011), A close encounter with a Saturn kilometric radiation source region, in *Proceedings of the 7th International Workshop*

on Planetary, Solar and Heliospheric Radio Emissions (PRE VII), edited by H. O. Rucker et al., pp. 75–85, Austrian Academy of Sciences Press, Vienna, Austria.

Lamy, L., P. Zarka, B. Cecconi, R. Prangé, W. S. Kurth, and D. A. Gurnett (2008a), Saturn kilometric radiation: Average and statistical properties, *J. Geophys. Res.*, *113*, A07201, doi:10.1029/2007JA012900.

Lamy, L., B. Cecconi, R. Prangé, P. Zarka, J. D. Nichols, and J. T. Clarke (2009), An auroral oval at the footprint of Saturn's kilometric radio sources, colocated with the UV aurorae, *J. Geophys. Res.*, *114*, A10212, doi:10.1029/2009JA014401.

Lamy, L., et al. (2010), Properties of Saturn kilometric radiation measured within its source region, *Geophys. Res. Lett.*, *37*, L12104, doi:10.1029/2010GL043415.

Lamy, L. (2011), Variability of southern and northern SKR periodicities, in *Proceedings of the 7th International Workshop on Planetary, Solar and Heliospheric Radio Emissions (PRE VII)*, edited by H. O. Rucker et al., pp. 38–50, Austrian Academy of Sciences Press, Graz, Austria.

Le Quéau, D., and P. Louarn (1989), Analytical study of the relativistic dispersion: Application to the generation of the auroral kilometric radiation, *J. Geophys. Res.*, *94*(A3), 2605–2616, doi:10.1029/JA094iA03p02605.

Masters, A., J. P. Eastwood, M. Swisdak, M. F. Thomsen, C. T. Russell, N. Sergis, F. J. Crary, M. K. Dougherty, A. J. Coates, and S. M. Krimigis (2012), The importance of plasma β conditions for magnetic reconnection at Saturn's magnetopause, *Geophys. Res. Lett.*, *39*, L08103, doi:10.1029/2012GL051372.

Menietti, J. D., R. L. Mutel, P. Schippers, S.-Y. Ye, D. A. Gurnett, and L. Lamy (2011), Analysis of Saturn kilometric radiation near a source center, *J. Geophys. Res.*, *116*, A12222, doi:10.1029/2011JA017056.

Morioka, A., et al. (2008), AKR breakup and auroral particle acceleration at substorm onset, *J. Geophys. Res.*, *113*, A09213, doi:10.1029/2008JA013322.

Morioka, A., Y. Miyoshi, F. Tsuchiya, H. Misawa, K. Yumoto, G. K. Parks, R. R. Anderson, J. D. Menietti, and F. Honary (2009), Vertical evolution of auroral acceleration at substorm onset, *Ann. Geophys.*, *27*, 525–535, doi:10.5194/angeo-27-525-2009.

Morioka, A., et al. (2010), Two-step evolution of auroral acceleration at substorm onset, *J. Geophys. Res.*, *115*, A11213, doi:10.1029/2010JA015361.

Morioka, A., et al. (2011), On the simultaneity of substorm onset between two hemispheres, *J. Geophys. Res.*, *116*, A04211, doi:10.1029/2010JA016174.

Morioka, A., Y. Miyoshi, N. Kitamura, H. Misawa, F. Tsuchiya, J. D. Menietti, and F. Honary (2012), Fundamental characteristics of field-aligned auroral acceleration derived from AKR spectra, *J. Geophys. Res.*, *117*, A02213, doi:10.1029/2011JA017137.

Mutel, R. L., J. D. Menietti, D. A. Gurnett, W. Kurth, P. Schippers, C. Lynch, L. Lamy, C. Arridge, and B. Cecconi (2010), CMI growth rates for Saturnian kilometric radiation, *Geophys. Res. Lett.*, *37*, L19105, doi:10.1029/2010GL044940.

Nichols, J. D., et al. (2009), Saturn's equinoctial auroras, *Geophys. Res. Lett.*, *36*, L24102, doi:10.1029/2009GL041491.

Provan, G., D. J. Andrews, B. Cecconi, S. W. H. Cowley, M. K. Dougherty, L. Lamy, and P. M. Zarka (2011), Magnetospheric period magnetic field oscillations at Saturn: Equatorial phase "jitter" produced by superposition of southern and northern period oscillations, *J. Geophys. Res.*, *116*, A04225, doi:10.1029/2010JA016213.

Rucker, H. O., et al. (2008), Saturn kilometric radiation as a monitor for the solar wind?, *Adv. Space Res.*, *42*, 40–47.

Russell, C. T., and R. L. McPherron (1973), Semiannual variation of geomagnetic activity, *J. Geophys. Res.*, *78*, 92–108, doi:10.1029/JA078i001p00092.

Schippers, P., et al. (2011), Auroral electron distributions within and close to the Saturn kilometric radiation source region, *J. Geophys. Res.*, *116*, A05203, doi:10.1029/2011JA016461.

Talboys, D. L., E. J. Bunce, S. W. H. Cowley, C. S. Arridge, A. J. Coates, and M. K. Dougherty (2011), Statistical characteristics of field-aligned currents in Saturn's nightside magnetosphere, *J. Geophys. Res.*, *116*, A04213, doi:10.1029/2010JA016102.

Tao, C., R. Kataoka, H. Fukunishi, Y. Takahashi, and T. Yokoyama (2005), Magnetic field variations in the Jovian magnetotail induced by solar wind dynamic pressure enhancements, *J. Geophys. Res.*, *110*, A11208, doi:10.1029/2004JA010959.

Taubenschuss, U., H. O. Rucker, W. S. Kurth, B. Cecconi, P. Zarka, M. K. Dougherty, and J. T. Steinberg (2006), Linear prediction studies for the solar wind and Saturn kilometric radiation, *Ann. Geophys.*, *24*, 3139–3150.

Tokumaru, M., M. Kojima, and K. Fujiki (2012), Long-term evolution in the global distribution of solar wind speed and density fluctuations during 1997–2009, *J. Geophys. Res.*, *117*, A06108, doi:10.1029/2011JA017379.

Voots, G., D. A. Gurnett, and S.-I. Akasofu (1977), Auroral kilometric radiation as an indicator of auroral magnetic disturbances, *J. Geophys. Res.*, *82*, 2259–2266.

Wang, Y. M., E. Robbrecht, and N. R. Sheeley (2009), On the weakening of the polar magnetic field during solar cycle 23, *Astrophys. J.*, *707*, 1372–1386, doi:10.1088/0004-637X/707/2/1372.

Wang, Z., D. A. Gurnett, G. Fischer, S. Y. Ye, W. S. Kurth, D. G. Mitchell, J. S. Leisner, and C. T. Russell (2010), Cassini observations of narrowband radio emissions in Saturn's magnetosphere, *J. Geophys. Res.*, *115*, A06213, doi:10.1029/2009JA014847.

Wu, C. S., and L. C. Lee (1979), A theory of the terrestrial kilometric radiation, *Astropys. J.*, *230*, 621–626.

Ye, S.-Y., D. A. Gurnett, G. Fischer, B. Cecconi, J. D. Menietti, W. S. Kurth, Z. Wang, G. B. Hospodarsky, P. Zarka, and A. Lecacheux (2009), Source locations of narrowband radio emissions detected at Saturn, *J. Geophys. Res.*, *114*, A06219, doi:10.1029/2008JA013855.

Zarka, P., L. Lamy, B. Cecconi, R. Prangé, and H. O. Rucker (2007), Modulation of Saturn's radio clock by solar wind speed, *Nature*, *450*, 265–267.

Zarka, P. (2004), Radio and plasma waves at the outer planets, *Adv. in Space Res.*, *33*, 2045–2060.